Intelligent Power Control of Inverter Air Conditioners in Power Systems: A Brain Emotional Learning-Based Approach

Oshnoei, Arman; Sadeghian , Omid ; Anvari-Moghaddam, Amjad

Published in:
I E E E Transactions on Power Systems

DOI (link to publication from Publisher):
DOI: 10.1109/TPWRS.2022.3218589

Publication date:
2022

Document Version
Accepted author manuscript, peer reviewed version

Intelligent Power Control of Inverter Air Conditioners in Power Systems: A Brain Emotional Learning-based Approach

Arman Oshnoei, *Member, IEEE*, Omid Sadeghian, *Student Member, IEEE*, and Amjad Anvari-Moghaddam, *Senior Member, IEEE*

***Abstract*—Inverter air-conditioning (IAC) units have been proved to be effective in frequency regulation by providing flexible capacities. This paper proposes a brain emotional learning (BEL)-based controller to provide the IACs with control signals to be efficiently involved in the frequency regulation in power systems. The BEL-based controller can learn quick-auto, making it appropriate in systems facing uncertainty. To assess the BEL controller performance in realistic conditions, the uncertainties as a consequence of variations in system parameters and load level are considered. The goal is to use the BEL controller to increase the IAC units' ability to track regulation signals accurately in uncertain circumstances. The controller is compared to a fuzzy-PI control, a proportional control scheme, a model predictive control and a linear quadratic regulator control. A delay-dependent stability criterion is used to calculate the highest time delay in the IACs response under which the system maintains stability. In addition, this paper presents an BEL-based coordinator to coordinate the IACs and traditional generation units for compensating considerable frequency variations caused by the time delays. Case studies are accomplished on a multi-area power system in MATLAB/Simulink environment. Eventually, real-time verifications by OPAL-RT real-time digital simulator on the simulated power system are executed to assess the control method.**

***Index Terms*—Inverter air conditioners, brain emotional learning, intelligent control, frequency control, multi-area power system.**

I. Introduction

A. Background and Motivation

FOLLOWING sudden changes in load value, the imbalance between generation and consumption must be redressed promptly to avoid severe frequency violations [1]. The traditional generation units (TGUs) are used conventionally to handle the frequency regulation. Nevertheless, TGUs may not be reliable, secure, and sufficient nowadays. This is because of the slow dynamic of TGUs' mechanical components, air pollution issues, and the high cost of regulation reserves by TGUs [2]. The next potential candidate for providing the regulation reserves is energy storage system (ESS). ESS devices, however, suffer from high capital cost and low efficiency [3]. Consequently, demand response (DR) can be recognized as a prospective candidate to sustain the system frequency over safety thresholds and decrease the additional reserves required from TGUs. The current advancement in data and communication technologies has facilitated the load side to involve in the frequency control under the DR plan [4]. It is achieved by turning the devices on/off or adjusting the consumption manners in reaction to control signals in a power grid [1]. Hardware demonstration for DR applications is provided in [5].

Heat pump water heaters (HPWPs), air conditioners (ACs), refrigerators, and plug-in electric vhicles (EVs) are among the most responsive loads to contribute to frequency regulation. The flexibility of EVs as movable ESSs is leveraged for primary frequency control (PFC) [6], and secondary frequency control (SFC). Provision of frequency support from HPWHs is verified in [7]. A study into how domestic refrigerators can fulfill the regulation requirements is considered in [8]. Among these appliances, the ACs have attracted much interest due to their controllability and little influence on the consumer comfort [9]. In the current market, ACs are classified into two types of fixed speed-based ACs (FSACs) and inverter-based ACs (IACs). A compressor is the main component of both AC types for power consumption. The fixed speed AC is only controllable by switching between ON or OFF modes of the compressor. On the contrary, the compressor of IACs is adjustable so that by changing the operating frequency of the IAC, the power consumption is controllable continuously [10]. The IACs installed at the load side are generally larger in number but smaller in capacity. Thus, they individually account for too small contributions to the network. The aggregation makes it possible to reach a higher power capacity compared to individual IACs. Substantial infrastructures are, however, needed to send the remote demand commands from control centers to the numerous IACs. By using wide area measurement system in power systems, a new challenge is emerged known as time delay in the delivery of regulation signals through communication links [12]. The time delay affects the regulation performance of the power systems with IACs. Hence, developing a coordination between IACs and TGUs seems essential. Besides, the power generation and consumption feature in smart grids require a frequency controller with robust performance and fast response-ability. Thus, an adaptive frequency controller for IACs is demanded to decrease the impact of various power imbalances.

B. Literature Review

Some investigations have been accomplished to study the usage of FSACs and IACs in the regulation services. In [13], a co-optimization approach of control capabilities and period

Arman Oshnoei and Amjad Anvari-Moghaddam are with the Integrated Energy Systems Lab, Department of Energy (AAU Energy), Aalborg University, 9220 Aalborg, Denmark, (emails: aros@energy.aau.dk, aam@energy.aau.dk).

Omid Sadeghian is with the Faculty of Electrical and Computer Engineering, University of Tabriz, Tabriz, (email: omidsadeghian@tabrizu.ac.ir).

time is proposed to alleviate the rebound of FSACs after contributing to regulation services. A priority-based control approach is presented in [14] to follow a control command based on the power need of FSACs units. However, these studies' regulation services provide operating reserves rather than PFC or SFC services. An FSACs operating power owns only two values, i.e., zero and rated capacity. Accordingly, when operating at the rated power, FSACs cannot increase their power usage. The IACs are more appropriate to provide regulation services for power grids as their operating power can be adjusted flexibly. In [15], an equivalent model for IACs is presented to support the system frequency by changing their setpoints. In [16] and [17], the IACs are employed to provide PFC service. In [9], a coordinated control strategy is proposed for IAC units to participate in SFC, which improves regulation service by enlarging the frequency reserve. In [9], IACs are equivalent to a conventional unit and can be regulated as a generator to support the frequency control. Studies on control strategies for IACs in SFC are limited to [18] and [19]. A model-based control strategy is presented in [18] for frequency control by the aggregated IACs. In [19], the authors suggest the allocation approach of control capabilities to schedule the IACs in numerous time scales in a power grid. In [20], the control and modeling methods of IACs to take part in power system frequency regulation is investigated.

Various control approaches are presented for the frequency control problem, including sliding mode control [21], linear quadratic regulation [22], fractional-order control [23], model predictive control [24], and fuzzy logic control [12]. Having the capability to handle the uncertainties and disturbances in complicated nonlinear systems, neural network and fuzzy logic methods are effective solutions greatly utilized in the frequency control studies of the power systems. In [12], a fuzzy-based approach is employed to deal with the control actions for the TGUs to respond to the regulation signals. The main challenge is the need for a precise strategy in producing membership functions and providing fuzzy rules. In [25], a method based on deep neural networks generates the control actions for the responsive units in a power system. Nevertheless, this approach needs a lot of computations for the purpose of training. A model based on the emotional learning in the human brain's limbic system was developed [26]. This model, referred to as a brain emotional learning (BEL) model, is an efficacious controller for quick decision-making, especially in uncertain conditions.

Minimal calculation intricacy, the online learning ability, and no requirement for previous understanding of system dynamics make BEL a specific method in compatison to other intelligent methods. Also, it doesn't necessitate an additional iterative process for training [27]. The BEL is growingly being used in control engineering [28], electrical motors [29], and AC microgrids [30]. It is demnostrated in [31] that the BEL provides superior performance over neural network and fuzzy logic in stabilizing the power systems under fault. By creating a program in the "C" computer language, the BEL controller can be executed via software. The program is compiled using TI's "C" compiler, and the DSP processor then receives the produced code. For example, in [32], a TMS320C31 DSP floating-point processor is used to experimentally implement the BEL-based controller for synchronous motor drives. A DSP-based prototype system (TMS320F28335 signal processor board) is made in [33] to develop an experimental test-bed for synchronous reluctance motor drives controlled by BEL control. Besides, unlike the BEL-based control approach, meta-heuristic algorithms are only used as offline tuning approaches. This means that identifying the optimal parameters of a control scheme by these algorithms relies on operating conditions, which may affect the execution of the control system.

C. Research Gap and Contributions

In brief, a gap has been observed in the previous studies as follows:

(i) Existing research mainly concentrates on the IACs' modeling and dispatch methods, while the design of adaptive controllers to provide the IACs with the regulation commands for efficient contribution in the frequency regulation service has gained little consideration.
(ii) The control methods of IACs existing in the literature mostly depend on the operating conditions. In this case, unpredictable changes in the system's parameters impact the controller's execution.
(iii) Some technical issues could occur in the event of a delayed reaction or variable IAC interference. It is essential to establish collaboration between IACs and TGU to solve the following problems. No study has been conducted using a coordination strategy.
(iv) The performance of power grids with IACs may be impacted by various factors, including external disturbances, the uncertainty of parameters, and unknown dynamics. Therefore, the role of IACs in providing regulation capacities in the face of uncertainty requires more investigation.
(v) Providing a computationally efficient and model-free adaptive control method in the control loop of IACs taking uncertainty in generating the control commands into consideration has not been addressed in the literature.

Also, Table I summarizes a taxonomy of existing publications addressing the use of IACs in providing frequency regulation services and compares them to highlight the main contributions of this paper.

To bridge the mentioned gaps, this paper proposes a BEL-based adaptive controller to provide proper frequency regulation signal tracking by the aggregated IACs in a multi-area power system. The proposed controller gives the ability to deal with the uncertainties affected by parameters changes and loads fluctuations in the system. The controller's convergence conditions are also studied. The controller is compared to a fuzzy-PI control, a proportional control scheme, and MPC and LQR-based control schemes. In addition, the impact of the delayed response of the IACs is assessed by using a delay-dependent stability criterion to calculate the highest time delay under which the system with IACs maintains stability. An intelligent supervisory coordinator is also proposed to make a coordination between the IAC aggregators and TGUs to remove excess generation, which can be created/removed

TABLE I
COMPARISON BETWEEN THIS PAPER'S CONTRIBUTIONS AND THOSE OF PREVIOUS STUDIES

Refs.	Control method		Coordination between IACs and CGU	Uncertainty consideration	Communication delay	Robust stability criterion
	Model-based	Model-free				
[9]	✓	–	–	–	✓	–
[10]	✓	–	–	–	–	–
[16]	✓	–	–	–	–	–
[17]	✓	–	–	–	–	–
[18]	✓	–	–	✓	✓	–
[19]	✓	–	–	–	–	–
[20]	✓	–	–	✓	✓	–
This paper	✓*	✓	✓	✓	✓	✓

*: For comparison purposes

during lengthy delays. The design is such that the BEL coordinator produces supplementary gains for the classic controller embedded in the control loop of TGUs based on the measured power information from the IACs and Area Control Error (ACE).

II. PROPOSED LFC SCHEME

A. Control framework of IACs

A control structure for participation of IACs in regulation service is depicted in Fig. 1. For the provision of reserve capacities by IACs, as illustrated in the figure, the entities, including the consumers, the aggregators, and the system operator, are involved [34]. The consumers, who get involved in the DR programs, sign contracts on altering the consumption manner in reaction to control commands in the power system. Depending on a DR plan's special form and type, the aggregators can be load-serving entities, distribution grid operators, or DR suppliers. During the system contingency, the system operator provides a signal containing the frequency and tie-line power changes designated as ACE and transmits it to the aggregators. The aggregators would then distribute the control command among the IACs according to the number of available devices in continuous-time domain. Upon receiving the control signal, the IACs change the operating frequency so that the electricity consumption of the IACs is controllable continuously. It is supposed that the IACs are provided with smart controllers, which allow the consumers to adjust the parameters, such as control modes, controllable periods, and temperature ranges[35]. We have assumed an electricity system design where the system operators are in charge of ensuring reliable and safe system operation and must ultimately ensure a balance between consumption and generation. Moreover, we assume that the IAC devices can measure the frequency with the necessary precision and apply the control command as quickly as needed. Keep in mind that this architecture necessitates very minimal communication between aggregators and devices. Each device will communicate the data to the aggregator, instructing the devices to activate their reserves. This attractive aspect of the suggested architecture significantly reduces whole communication.

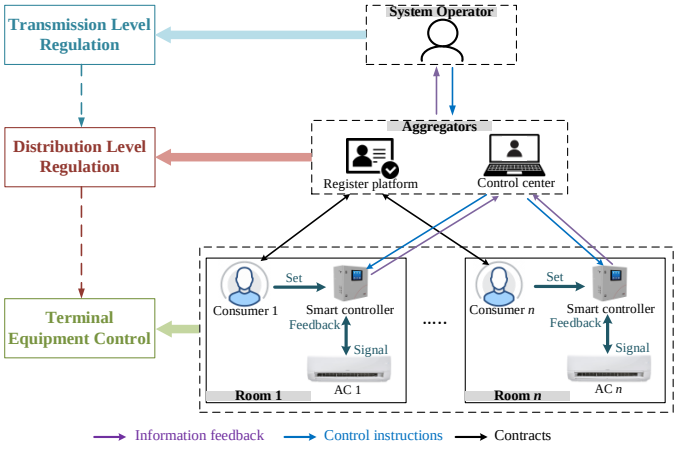

Fig. 1. Control structure for the participation of IACs in frequency control

B. Reserve capability of IACs

To derive the power output of IAC aggregators according to the regulation signal, an equivalent model of IACs is required in the frequency control problem. The mathematical model of an IAC should be extracted from thermal and electrical models. The thermal model in the time domain is mathematically expressed as follows [19]:

$$\rho_d M_r V_r \frac{\mathrm{d}\theta_r(t)}{\mathrm{d}t} = Q_r(t) - Q_{IAC}(t) \tag{1}$$

As (1) implies, the room's thermal model is expressed by the relationship between the room thermal deviation and room temperature (θ_r). The thermal deviation is indicated based on the room's heat gain (Q_r) and the IACs refrigerating capacity (Q_{IAC}). In (1), the notations M_r and ρ_d, represent the heat capacity of the air and density, respectively; and V_r denotes the volume of the room.

The heat gain of the room is derived from the heat transfer between outdoor and indoor air as follows:

$$Q_r(t) = E_{tc}\left(\theta_0(t) - \theta_r(t)\right) \tag{2}$$

where E_{tc} represents equivalent thermal conductance between the outdoor and room air. The main feature of IAC is the operating frequency which is adjustable to change the compressor speed. The electrical model of IAC is, therefore, generated

based on the operating frequency. By regulating the frequency, the operating power (P_{IAC}) and refrigerating capacity (Q_r) of the IAC can be controlled as follows:

$$P_{IAC}(t) = p(t) f_{IAC}(t) + c_{p2} \tag{3}$$

$$Q_{IAC}(t) = q(t) f_{IAC}(t) + c_{q2} \tag{4}$$

where

$$p(t) = \frac{c_{p1}}{T_c} e^{\frac{-1}{T_c} t}; \quad q(t) = \frac{c_{q1}}{T_c} e^{\frac{-1}{T_c} t} \tag{5}$$

where c_{p1}, c_{p2}, c_{q1}, and c_{q2} are constant factors of the IAC; and T_c is the compressor's time constant. The operating frequency of IAC (f_{IAC}) can be controlled in a defined range as follows:

$$f_{IAC}^{\min} \leq f_{IAC} \leq f_{IAC}^{\max} \tag{6}$$

where the bound values $f_{IAC}^{\min}$ and $f_{IAC}^{\max}$ represent, respectively, the minimum and maximum operating frequencies.

In a normal case, without participation in regulation process, the operating frequency of IAC is controlled based on the difference between the room temperature (θ_r) and the set temperature (θ_{st}) of the IAC, which can be expressed as:

$$\Delta f_{IAC}(t) = a\theta_{dev}(t) + b \int \theta_{dev}(t) dt \tag{7}$$

$$\theta_{dev}(t) = \theta_r(t) - \theta_{st}(t) \tag{8}$$

To take part in the regulation service, the operating power and frequency of IAC should be adjusted according to the ACE deviations. To achieve this aim, a control signal (u_{IAC}) from the central control center is provided to the aggregated IACs in the system to regulate the operating power. This control signal is produced by monitoring the frequency and tie-line deviations in power areas of the power system. Hence, equation (7) can be rewritten as follows:

$$\Delta f_{IAC}(t) = u_{IAC}(t) + a\theta_{dev}(t) + b \int \theta_{dev}(t) dt \tag{9}$$

By considering above equations in the thermal and electrical models of IAC, the operating power change of the IAC in response to the regulation signal of power system can be expressed as follows:

$$\Delta P_{IAC}(t) = c_{p1} \Delta f_{IAC}(t) \tag{10}$$

$$P_{IAC}(t) = c_{p1}\left(u_{IAC}(t) + a\left(\theta_r(t) - \theta_{st}\right) + b\int \left(\theta_r(t) - \theta_{st}\right) dt \right) \tag{11}$$

As (11) illustrates, the operating power of the IAC is changed by the deviations of the set temperature of the IAC, the temperature in the room, and the regulation signal. Since the IAC operating power should be controlled in a short time for the regulation purpose, it is convincing to suppose that the IAC set remains constant in such a short period [19].

$$\Delta\theta_{st} \cong 0 \tag{12}$$

Therefore, equation (11) can be simplified as follows:

$$\Delta P_{IAC}(t) = c_{p1}\left(u_{IAC}(t) + a\theta_r(t) + b \int \theta_r(t) dt \right) \tag{13}$$

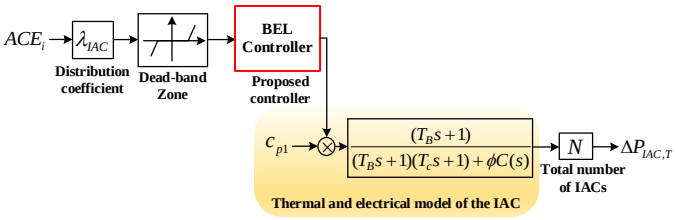

Fig. 2. Transfer function model of aggregated IACs

It is obvious from (13) that the operating power of IAC can be adjusted according to the control commands sent from the controller.

From equation (1) to (13), the IAC power can be represented in the frequency domain as follows:

$$\Delta P_{IAC}(s) = \frac{c_{p1}(T_B s + 1)}{(T_B s + 1)(T_c s + 1) + \phi C(s)} u_{IAC}(s) \tag{14}$$

where

$$T_B = \frac{\rho_d M_r V_r}{E_{tc}}; \quad \phi = \frac{c_{q1}}{E_{tc}} \tag{15}$$

The IAC's internal temperature controller, $C(s)$, allows users to change the running frequency and maintain a constant indoor temperature to meet its setpoint and can be developed by a PI controller as follows:

$$C(s) = a + \frac{b}{s} \tag{16}$$

where a and b represents the gains of PI controller.

IACs control loop includes an operational constraint to ensure the users' comfort. This constraint is formulated as follows [9]:

$$|\Delta P_{IAC}| \leq \frac{c_{p1} \Delta\theta_{r,max}}{\phi} \tag{17}$$

This equation implies that as long as the operating power change of the IAC ΔP_{IAC} is less than $\Delta\theta_{r,max}$, the indoor temperature deviation satisfies the temperature boundary value permitted by the users. Consequently, the setting value of $\Delta\theta_{r,max}$ should be carefully considered to balance the regulation performance and consumer comfort.

The transfer function model of aggregated IACs is shown in Fig. 2. The model comprises a thermal and electrical model taken from [19] and secondary control with the proposed BEL-based adaptive controller. The output power change of the IAC aggregator, which is in charge of supervising N distributed IACs, is expressed as

$$\Delta P_{IAC,T} = \sum_{l=1}^{N} \Delta P_{IAC_l}. \tag{18}$$

The limitations on the aggregator operating power are accordingly chosen from the limits on the operating power of the IACs (i.e. (17)).

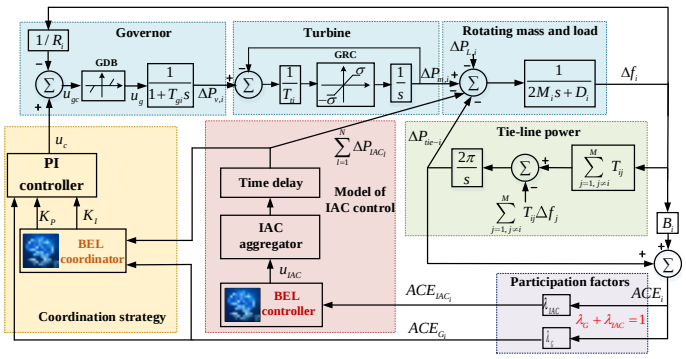

Fig. 3. System frequency response model with IAC

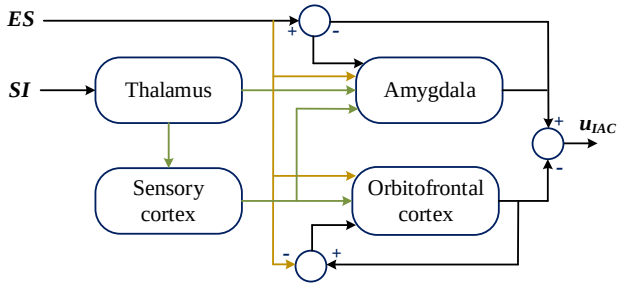

Fig. 4. Structure of BEL controller

III. Frequency Response Model of Power System with IACs

Since the AGC operation involves little variations, thus each control area of a power grid is modeled by an equivalent generator with a turbine, a governor, and an AGC system. Besides, the time constant of automatic voltage regulator (AVR) loop is shorter than the AGC; thus, it is possible to dissociate the AGC loop from the AVR loop [36]. Thus, reliable LFC studies can be performed using a linear model of the AGC system [36][37]. Fig. 3 illustrates the block diagram for the control area i with IAC control. The variation in frequency deviation in area i can be described as

$$\Delta \dot{f}_i = -\frac{D_i}{2M_i}\Delta f_i - \frac{1}{2M_i}\left(\Delta P_{L_i} - \Delta P_{m,i} + \sum_{l=1}^{N}\Delta P_{IAC_{l,i}} + \Delta P_{tie-i}\right) \tag{19}$$

where ΔP_{L_i} and ΔP_{m_i} are the changes in the load, and in the generation of TGU, respectively; M_i and D_i represent the inertia constant of TGU and the load damping coefficient, respectively; and ΔP_{tie_i} is the change in the overall power flowing across the tie lines spanning area i and nearby areas.

The nonlinear characteristic associated with the governor dead band (GDB) is incorporated into the model, which can be expressed as follows:

$$u_g(t) = \max(0, u_{gc} - u_{gc_0}) + \min(0, u_{gc} + u_{gc_0}) \tag{20}$$

where the operators *max* and *min* return the maximum and minimum value of their arguments, respectively; $\pm u_{gc_0}$ represent the bounds of the dead zone; and u_{gc} denotes the provided signal for the governor, which is calculated as follows:

$$u_{gc} = u_c - \frac{\Delta f_i}{R_i} \tag{21}$$

where u_c is the produced signal by the controller, and R is the speed adjustment factor. The impact of the generation rate constraint (GRC) on the turbine power can be modeled as follows:

$$P_m = \int [\min\left(\max(0, \frac{\mathrm{d}P'_{m,i}}{\mathrm{d}t}), \sigma\right) + \max\left(\min(0, \frac{\mathrm{d}P'_{m,i}}{\mathrm{d}t}), -\sigma\right)]\mathrm{d}t \tag{22}$$

where P'_m denotes the input signal to the GRC block, and $\pm\sigma$ are the maximum and minimum allowed values for the generation rate.

The IACs are assumed to participate in the LFC based on the provided ACE_{IAC}. The IAC bypasses the signal unless its value exits a dead zone of a positive upper bound and a negative lower bound. The IACs are needed to decrease the power consumption when ACE_{IAC} drops below the lower bound and increase the power consumption when it surpasses the upper bound. This control process holds on the condition that the room temperature for each IAC is within the permitted range of variation $\Delta\theta_{r,max}$. With the restoration of the system frequency, the IACs' operational frequencies will return to their initial settings; hence the frequency regulation service has slight or no influence on the customers' convenience in the short period for the LFC [9].

IV. Design of Controller for IAC aggregator

A BEL-based controller is proposed in this paper to generate the control commands for the aggregated IACs to contribute to frequency regulation service. The controller is formed of Amygdala, which is involved in emotional learning, sensory cortex, Thalamus, and Orbitofrontal cortex [38]. Sensory input (S) and emotional signal (E) are the model inputs. A simplified structure of the BEL used in this work is depicted in Fig. 4. A and O networks express the blocks associated with the amygdala and orbitofrontal cortex, respectively. The BEL output is obtained based on the subtraction of network A and network O outputs, represented by

$$u_{IAC}(t) = A(t) - O(t). \tag{23}$$

The S and E are the A network inputs. Section III-B discusses the selection process for S and E. The A network output is represented by [30], [38]:

$$A(t) = S(t)Z(t) \tag{24}$$

where $Z(t)$ is a connection weight, which is given as follows:

$$Z(t) = \int_0^t \delta z(t)dt + Z(0) \tag{25}$$

where

$$\delta z(t) = \alpha S(t)[max(0, E(t) - A(t) - A_c(t)) \tag{26}$$

$$A_c(t) = max[S(t)]Z_c(t) \tag{27}$$

where α represents the learning rate; Ac is a neuron with the greatest amount of sensory input; $max[S]$ denotes the greatest of all sensory signals. The Z_c is described by:

$$Z_c = \int_0^t \delta z_c dt + Z_c(0). \tag{28}$$

The S and E together with the prior model output are the O network inputs. The network O output is calculated as follows:

$$O(t) = S(t)P(t) \tag{29}$$

where $P(t)$ is a connection weight that change as:

$$P(t) = \int_0^t \delta p(t) dt + P(0) \tag{30}$$

where

$$\delta p(t) = \beta S(t)[A(t) - O(t) - E(t)] \tag{31}$$

where β is the inhibition rate; eventually, the BEL output in (23) is given by:

$$\begin{aligned} u_{IAC}(t) = S(t)[\alpha \int_0^t S(t)[max(0, E(t) - A(t) - A_c(t))]dt \\ - \beta \int_0^t S(t)[A(t) - O(t) - E(t)]dt]. \end{aligned} \tag{32}$$

The following section discusses the convergence conditions.

A. Convergence condition

Theorem 1. *Given the controller's weight adjustments as in (23) to (31), there is a synthesis of S signal, α and β parameters such that [30], [38]*

$$1)|1 - \alpha S(t)^2| < 1$$
$$2)|1 - \beta S(t)^2| < 1$$

Which guarantees the weights' asymptotic convergence associated with A and O networks.

Proof. The BEL controller's actions is examined in two different periods, namely the transient and steady-state periods. At first, for the transient period, (26) can be written as:

$$\delta z(t) = \alpha S(t)[E(t) - A(t) - A_c(t)] \tag{33}$$

In the steady-state period, there is zero weight variation in the A and O networks. i.e.

$$\delta z(t) = \delta z_c(t) = \delta p(t) = 0 \tag{34}$$

Assuming $S(t) \neq 0$, and applying the condition (34) on (33) and (31)

$$E(t) = A_c(t) = S(t)Z_c(t) = u_{IAC}(t) \tag{35}$$

where z_c and z_c^* are the weight of network A during and after adjustment, respectively; and $E'(t) = S(t)Z_c(t)$ and $E' = S(t)Z_c^*$ are E signal prior to and following adjustment, respectively. The following is the weight adjustment for δz_c:

$$\delta z_c(t) = \alpha S(t)[max(0, (E(t) - E'(t))] \tag{36}$$

when $E(t) - E' > 0$, (36) decreases to

$$\begin{aligned} \mu z_c(t) &= \alpha S(t)(E(t) - E') \\ &= \alpha S(t)\left(S(t)z_c^*(t) - S(t)Z_c(t)\right) = \alpha S^2(t)\tilde{Z}_c(t) \end{aligned} \tag{37}$$

where, $\tilde{Z}_c(t) = Z_c^*(t) - Z_c(t)$. $Z_c(t)$ changes during a brief period of δt as follows.

$$\begin{aligned} Z_c(t + \delta t) &= Z_c(t) + \delta z_c(t) \\ \tilde{Z}_c(t + \delta t) &= Z_c^*(t + \delta t) - Z_c(t + \delta t) \\ &= Z_a^*(t + \delta t) - Z_c(t) - \delta z_c(t) = (1 - \alpha S^2)\tilde{Z}_c(t) \end{aligned} \tag{38}$$

Therefore, $\tilde{Z}_c(t + \delta t) \rightarrow \tilde{Z}_c(t)$ if $|1 - \alpha S^2| < 1$. The change in Network O is represented as

$$\begin{aligned} \delta p(t) &= \beta S(t)(A(t) - O(t) - E(t)) \\ &= \beta S(t)\left(0 - S(t)P(t) - S(t)Z_c^*(t)\right) \\ &= -\beta S^2(t)\left(Z_c^*(t) + P(t)\right) = -\beta S^2(t)\tilde{P}(t) \end{aligned} \tag{39}$$

where $\tilde{P}(t) = Z_c^*(t) + P(t)$. The term $P(t)$ changes as

$$\begin{aligned} P(t + \delta t) &= P(t) + \delta p(t) \\ \tilde{P}(t + \delta t) &= Z_c^*(t + \delta t) + P(t + \delta t) \\ &= P_c^*(t + \delta t) + P(t) + \delta p(t) = (1 - \beta S^2)\tilde{P}(t) \end{aligned} \tag{40}$$

Therefore, $\tilde{P}(t + \delta t) \rightarrow \tilde{P}(t)$ if $|1 - \beta S^2| < 1$.

Remark I. *When selecting α and β, the convergence criteria covered in Theorem 1 should be taken into account.*

B. Design of S and E

To attain the favorable performance of the BEL-based controller, constituting a relation between S, E and controller output (u_{IAC}) is essential. The S and E inputs are selected as (41) and (42) respectively.

$$S = \phi_1 ACE_{IAC} + \phi_2 \int ACE_{IAC} dt \tag{41}$$

$$E = \gamma_1 ACE_{IAC} + \gamma_2 \int ACE_{IAC} dt + \gamma_3 u_{IAC} \tag{42}$$

where $ACE_{IAC} = \lambda_{IAC} ACE$ represents the ACE signal provided for the IAC aggregator; λ_{IAC} represents participation factor of IAC aggregator; ϕ_1 and ϕ_2 are weighting factors for the S function; and γ_1, γ_2, and γ_3 are weighting factors for the E function. Trial and error is used to determine the values of these weighting factors. The defined S and E functions are designed to achieve a quick reaction, the least amount of overshoot and steady-state error, and the least amount of deviation from a reference. Figure 5 displays the proposed control scheme for the aggregated IACs.

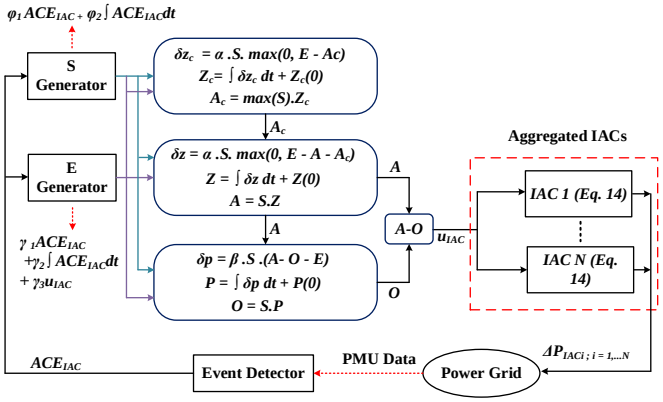

Fig. 5. Block diagram of the proposed BEL controller for the aggregated IACs

C. Control Bounds

This section aims to establish the necessary condition ensuring that the control command generated by the controller stays within the allowable boundaries. For a certain set-point change, this condition estimates the boundaries of the controller parameters and is applicable in all operating scenarios. The reference is set to a non-zero value, and it is assumed that the initial status is zero, then $ACE_{IAC} = y$. In this case, network A, network O, and A_c outputs are also starting at zero. However, the S function is non-zero. The first instant's control signal is calculated by (43) as $[E(0) - A(0) - A_0(0)] > 0$

$$u_{IAC}(t) = (\alpha + \beta)(\phi_1 + \phi_2)^2(\gamma_1 + \gamma_2)y^3 dt \tag{43}$$

where dt denotes the step-size. At this instant, network A and network O outputs are written as follows

$$A(1) = \alpha(\phi_1 + \phi_2)^2(\gamma_1 + \gamma_2)y^3 dt \tag{44}$$
$$O(1) = -\beta(\phi_1 + \phi_2)^2(\gamma_1 + \gamma_2)y^3 dt \tag{45}$$

There are two possibilities for the next instant's control signal. If $[E(1) - A(1) - A_0(1)] > 0$, then

$$u_{IAC}(2) = -S(1)^2[\beta((\alpha+\beta)(\phi_1+\phi_2)^2(\gamma_1+\gamma_2)y^3 - E(1))dt] \tag{46}$$

And, if $[E(1) - A(1) - A_0(1)] < 0$, then

$$u_{IAC}(2) = [S(1)^2\alpha(E(1) - 2\alpha(\phi_1+\phi_2)^2(\gamma_1+\gamma_2)y^3 - E(1))dt - \beta((\alpha+\beta)(\phi_1+\phi_2)^2(\gamma_1+\gamma_2)y^3 - E(1))dt] \tag{47}$$

It can be seen that the term $(\alpha + \beta)(\phi_1 + \phi_2)^2(\gamma_1 + \gamma_2)y^3 dt$ appears recurrently in consecutive iterations, and thus, maintaining the control command inside the saturation range is dependent on this term. Consequently, thanks to (48), the control command is kept within the saturation boundaries.

$$u_{IAC,min} \leq (\alpha + \beta)(\phi_1 + \phi_2)^2(\gamma_1 + \gamma_2)y^3 dt \leq u_{IAC,max} \tag{48}$$

where $u_{IAC,min}$ and $u_{IAC,max}$ denote the controller output's minimum and maximum values.

V. Coordination of IAC Aggregator and TGU under Communication Delays

The main feature of the aggregated IACs in this study is to contribute to frequency control in case of disturbances such as a step change in load of power system. However, as the majority of DR initiatives are contractually based and voluntary, therefore IAC participation in LFC may change over time. As a result, in the event of a delayed reaction or varied interference of IACs, several technical issues may arise. In other words, if the IAC aggregator' action is associated with time latency, TGU starts to restore the power balance via increasing/decreasing its generation level. Subsequently, the IAC aggregator is interfered as a supplementary control to compensate all or part of the power imbalance. In this case, the contribution of the TGU during the time delay may result significant frequency changes. In some cases with a large time delay, this could also impose instability to the power system performance. In such a condition, even if the frequency deviations do not jeopardize the power system performance, the excessive useless power generation by the TGU would consume a remarkable amount of fuel which means a substantial CO2 emission.

In this work, a BEL supervisory coordinator is presented to deal with the time delay in the power system with IACs. In other words, the BEL is designed to tackle the challenge of the frequency overshoots/undershoots derived by the inconsistency between the IAC aggregator and TGU and consequently, reducing CO2 emission and adjusting the TGU according to the regulation amount provided by the aggregated IACs. Hence, the BEL is not only used to produce the control actions for the IAC aggregator (as discussed in Section III), but also to coordinate the TGU and IAC aggregator. Figure 6 illustrates how the BEL-based coordinator is used to make the coordination between aggregator and TGU. As shown, the coordinator is provided with ΔP_{IAC} and ACE_G to cover the communication delay effect. The outputs are the parameters of the PI controller in the control loop of TGU. In other words, the BEL is used for the online tuning of PI controller parameters. Thus, this control arrangement offers a smooth execution in starting and unstable conditions. The input functions used in the BEL coordinator are given as:

$$S' = \phi_1' \Delta P_{IAC} + \phi_2' \int \Delta P_{IAC} dt \tag{49}$$

$$E' = \gamma_1' ACE_G + \gamma_2' \int ACE_G dt + \gamma_3' C_s \tag{50}$$

where S' and E' refer to the BEL coordinator's sensory and emotional signals, respectively; C_s is the output control signal of the coordinator; $ACE_G = \lambda_G ACE$ denotes the ACE signal provided for the TGU; and λ_G is participation factor of TGU. The weighting factors ϕ_1', ϕ_2', γ_1', γ_2', and γ_3', as in (49) and (50), are calculated via trial and error. Two scaling coefficients (SCs) are included in the coordinator structure to normalize the outputs. The following performance index is minimized by particle swarm optimization algorithm to tune the SCs.

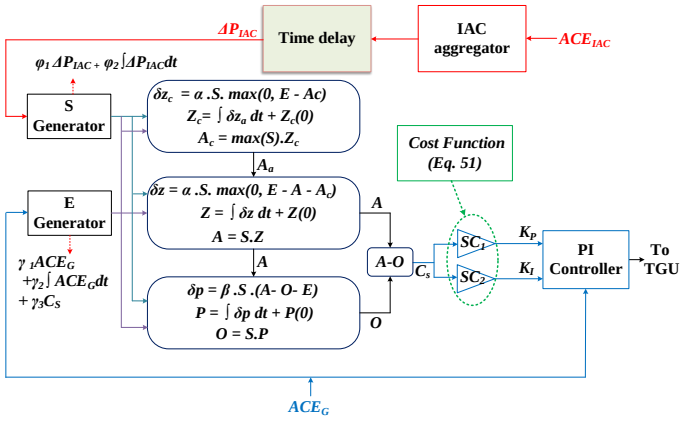

Fig. 6. Schematic of the proposed supervisory coordinator

$$\min \int_0^{T_{sim}} |\Delta f(t)|\, \mathrm{d}t \tag{51}$$

subject to

$$SC_{i,min} \leq SC_i \leq SC_{i,max} \qquad i = 1, 2 \tag{52}$$

where Δf represents the system frequency deviation; and T_{sim} is the length time of Δf.

Remark II. *Calculating the scaling coefficients and carrying out the coordination are the two steps that make up the proposed BEL supervisory coordinator. Because the coefficients are adjusted offline, the time and intricacy of the calculations are not highly valued. The coordination is conducted online, but it's a straightforward distribution of the responsive units. It means that it needs no control and analysis studies, and the coordination is carried out by using the scaling coefficients already computed offline.*

VI. Stability Analysis of the Proposed LFC Scheme

Considering the delays in the IAC aggregator control loop and neglecting the nonlinearities associated with the GDB and GRC in the generator control loop, the closed-loop model of the LFC system with IACs can be expressed from Fig. 2 and Fig. 3, as follows:

$$\frac{\mathrm{d}(x(t))}{\mathrm{d}t} = Ax(t) + B_G u_{gc}(t) + B_E u_{IAC}(t - \eta_k) + Fd(t)$$
$$y(t) = C^T x(t) \tag{53}$$

where η_k is a time-varying delay limited by

$$0 \leq \eta_k(t) \leq \tau_k, \quad \frac{\mathrm{d}(\eta_k(t))}{\mathrm{d}t} \leq \gamma_k \leq 1 \quad k = 1, ..., n \tag{54}$$

where τ and γ are the upper bound and the upper variation rate of the time delay; $x = [\Delta f_i\ \Delta P_{tie-i}\ \Delta P_{m,i}\ \Delta P_{v,i}\ \Delta P_{IAC,T}\ \Delta P_a\ \Delta P_b]^T$ is the vector of state variables; $F = \Delta P_{L,i}$ represents a system disturbance; and ΔP_a and ΔP_b are presented as the supplementary variables to derive the system's linear state-space model.

A delay-dependent stability criterion is established for the proposed LFC scheme. This analysis aims at deriving an admissible delay margin such that the system can remain asymptotically stable for all time delays less than the admissible delay upper bound. Theorem 1 given in [39] is used to identify the delay margin.

The detailed execution process for delay margin calculation is outlined in the following steps.

1) Input the LFC system parameters, as well as the BEL parameters and initial delays, and compute the state-space equation given in (53).
2) Use Theorem 1 given in [39] to study the stability of the LFC system with assigned delays.
3) If the system stability is secured, increase the delays with a slight increment, and calculate the state-space equation again, then move to Step 2. Otherwise, the delay in the last iteration is selected as delay margin.

VII. Case Studies

A. Test System

The simulations are performed in New England 10-generator 39-bus test system as shown in Fig. 7 [40]. The test system is divided into three areas for frequency analysis. The system's parameters are listed in Table II. The generating units in each area have been replaced with equivalent single generating units with equivalent speed regulation parameters and inertia constants, which are represented as follows

$$M_{eqv} = \frac{M_1 S_1 + M_2 S_2 + ... + M_n S_n}{S_{system}} \tag{55}$$

where, $S_{system} = S_1 + S_2 + ... + S_n$

$$R_{eqv} = \frac{1}{\frac{1}{R_1}\frac{S_1}{S_{system}} + \frac{1}{R_2}\frac{S_1}{S_{system}} ... + \frac{1}{R_n}\frac{S_n}{S_{system}}} \tag{56}$$

where S_i, R_i, and M_i are the individual machine rating, speed regulation parameter and inertia constant of generator i.

In order to ensure the safe operation of power generation equipment, the nonlinear generation rate constraint of governor is considered with rising/falling slew rates, and it is specified as 10% per minute (0.0017 p.u. MW/s). Also, the upper and lower bounds of dead zone for ACE_G are assumed to be $\pm$ 0.01 p.u. It is assumed that two IAC aggregators are included in areas 1 and 2 containing 30,000 IACs. The IACs available in each aggregator are assumed to have identical specifications and initial states. The parameters of the thermal and electric model of IACs are given in Table III [19]. A generalized LFC model for area i with the IAC aggregator is shown in Fig. 3. The IACs are all installed in the same area; hence, the respective area's tie-lines, frequency deviations, and equivalent constants are considered. The ACE signal in each area is allocated to the TGU and IAC aggregator using participation factors of 0.6 and 0.4, respectively. For the design of both BEL controller and BEL coordinator, the gains and weighting factors in (41), (42), (49), and (50) are as follow: $\alpha = 0.87$, $\beta = 0.95$, $\phi_1 = 1.70$, $\phi_2 = 1.40$, $\gamma_1 = 1.35$, $\gamma_2 = 1.00$, $\gamma_3 = 1.30$, $\alpha' = 0.70$, $\beta' = 0.80$, $\phi_1' = 1.70$, $\phi_2' = 1.40$, $\gamma_1' = 1.50$, $\gamma_2' = 1.95$, $\gamma_3' = 0.95$. The values of SCs are obtained as: $SC_1 = 0.67$ and $SC_2 = 0.77$.

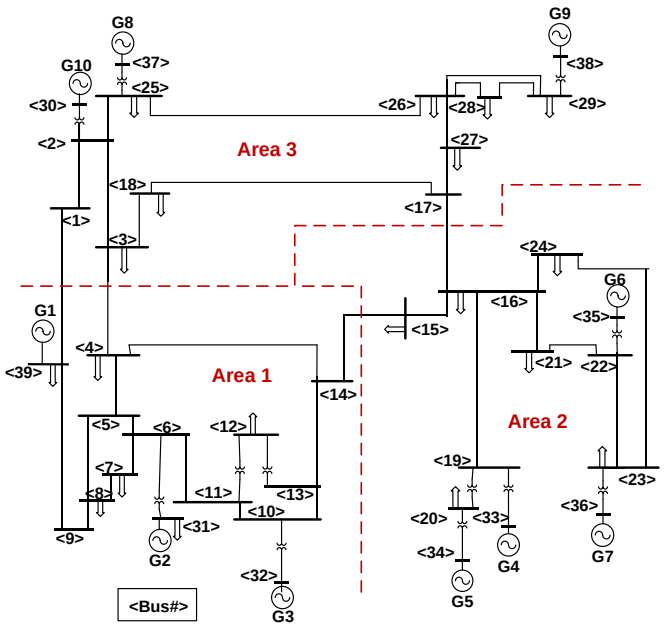

Fig. 7. Single-line diagram of test system

TABLE II
IEEE 39 BUS SYSTEM PARAMETERS [41]

Area No.	Unit No.	M	R	D	T_g	T_t
Area 1	1	4	3	0.0083	0.08	0.4
	2	3.5	3	0.0083	0.08	0.4
	3	2.5	1.8	0.0083	0.08	0.4
Area 2	4	2.5	2.4	0.0083	0.08	0.4
	5	3	1.8	0.0083	0.08	0.4
	6	4	2.1	0.0083	0.08	0.4
	7	3	1.8	0.0083	0.08	0.4
Area 3	8	2	1.5	0.0083	0.08	0.4
	9	4.5	2.1	0.0083	0.08	0.4
	10	5	2.4	0.0083	0.08	0.4

TABLE III
PARAMETERS OF IACS

Parameter	Value	Unit	Parameter	Value	Unit
M_r	1.005	kJ/(kg.°C)	$f_{IAC}^{\min}$	150	Hz
V_r	250	m^3	c_{p1}	0.04	kW/Hz
ρ_d	1.205	kg/m^3	c_{p2}	0.02	kW
a	0.52	Hz/°C	c_{q1}	0.12	kW/Hz
b	0.032	Hz/(°C.s)	c_{q2}	-0.05	kW
$f_{IAC}^{\min}$	1	Hz	θ_{st}	25	°C

B. Dynamic evaluation of the proposed control scheme

A comparison study is carried out to examine how well the suggested BEL-based controller performs. To this end, the controller is compared to a proportional control method for IACs aggregators reported in [19] and a fuzzy-PI control. To apply the fuzzy-PI control to IAC aggregators in each area, a collection of fuzzy rules including 27 rules is utilized in the fuzzy block. The inputs to the fuzzy block are ACE_{IAC} and its derivative. The outputs are the parameters of PI controller in the control loop of IAC aggregator. The membership functions (MFs) for inputs are the trapezoidal ones to cover a broad area of changes in ACE_{IAC} and $d/dtACE_{IAC}$. In addition, the outputs MFs, which are the gains of PI controller, are determined based on the triangular form to raise the computations speed of the fuzzy control. The MFs are presented in Appendix.

The performance of the controllers is compared for multiple-step changes in the load as plotted in Fig. 8 (a). The comparison results of ACE deviations are plotted in Figs. 8 (b)-(d), respectively. As seen, when the IAC aggregators are equipped with the BEL-based controller, considerable decreases in the peak value and settling time of dynamic responses are achieved compared to a proportional control and a fuzzy PI control. From Fig. 8, it is evident that fuzzy control also can work. However, its performance may be affected due to the fixed design of fuzzy rules. Besides, since proportional control contains a constant gain, the variation in the operating point and the advent of uncertainties that enter as additive disturbances to the system dynamic model may lead to poor presentation in both performance and convergence speed. Figures 8 (e)-(f) represents the regulation power of the TGUs and IACs with the proposed controller. As the figure shows, the TGUs and IACs follow the load variations by changing the output powers. The IACs yield down-regulation capacity by increasing the power consumption and provide up-regulation capacity by decreasing the power consumption. It is also clear that after the aggregators achieve the necessary peak value, their regulating abilities start to wane and eventually level off at zero, which shows that the setpoints of IACs return to the initial values with the frequency restoration. To study the robustness of the proposed BEL controller embedded in the control loop IAC aggregators, uncertainties are included in the governor time constant (T_g) and the synchronizing torque coefficient of the tie-line connecting areas 1 and 3 (T_{13}). The parameters are increased from zero to forty percent of what they were in the original operational state. The absolute maximum deviation of frequency responses in all areas is illustrated in Fig. 9 for varying parameters. As the results show, the dynamic responses are lightly affected, resulting in a robust performance in case of the variation in T_g and T_{13}.

C. Efficacy of Supervisory Coordination Scheme on Regulation Performance

This subsection aims to prove how the proposed BEL-based coordinator scheme faces frequency contingencies impacted by time delay, which may threaten regulation performance in case of a high time delay. In order to analyze the effects of delay, the time delays between the transmission system operator (TSO), IACs, and control center are grouped together and recognized as a single delay. Figure 10 shows the absolute value of the maximum frequency deviations obtained by the proposed BEL controller under varying delays in the control loop of both IAC from 0 to 1.5 s. This analysis is conducted under a 0.25 p.u. load change in both area 1 and area 2. In Fig. 10, the system stability's permitted delay boundary is calculated as $\tau_1 = \tau_2 = 1.322$ s, with the time-varying rate assumed as $\gamma = 0.5$. The change in the frequency of areas is shown in Fig. 11 for two different time delays (before and after the delay margin). As seen, the frequency deviation is unstable for the $\eta_2 = \eta_2 = 1.5$ s due to the delay margin.

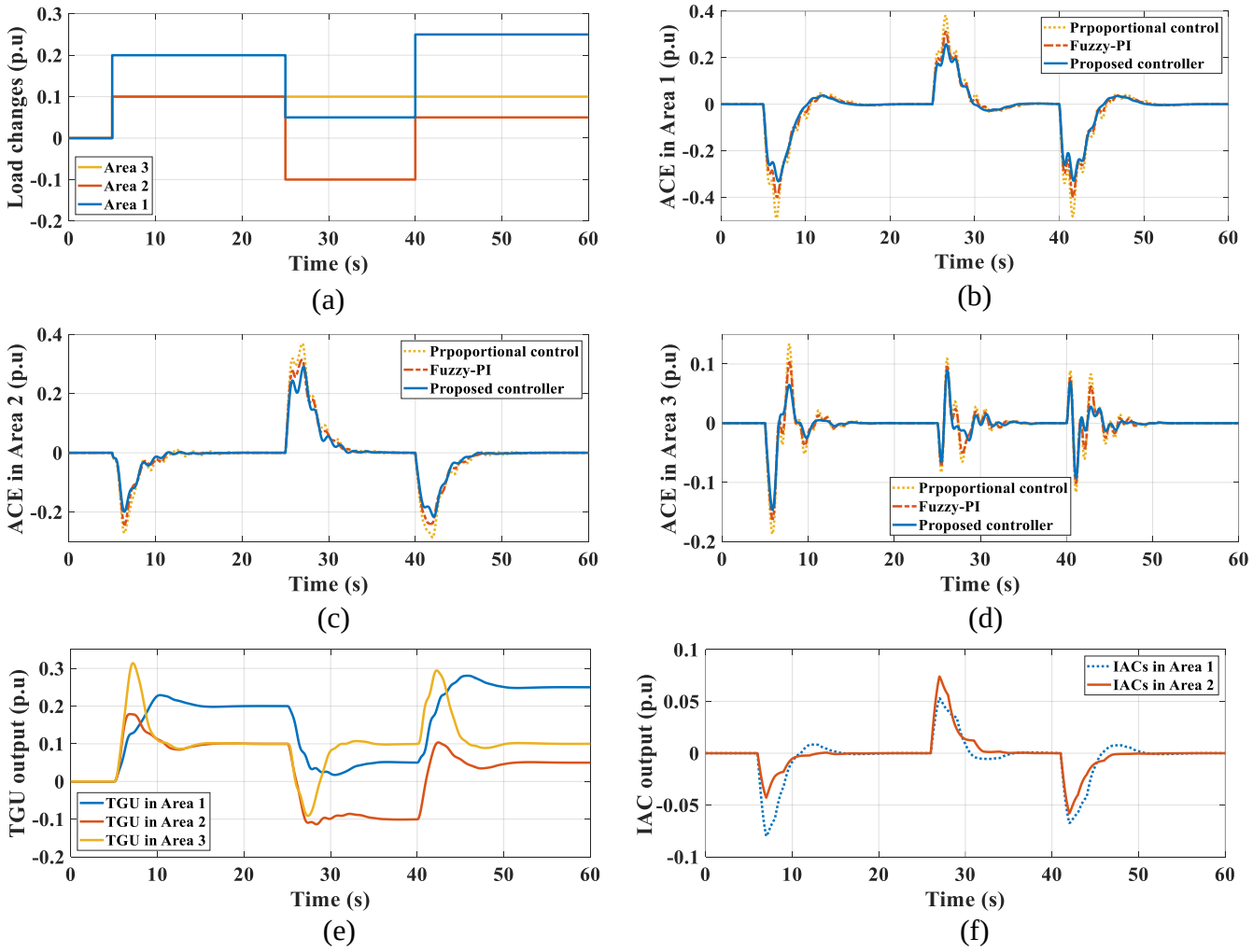

Fig. 8. (a) load change trend (b) ACE deviation in area 1; (c) ACE deviation in area 2; (d) ACE deviation in area 3; (e) regulating power of TGUs; (f) regulating power of IACs

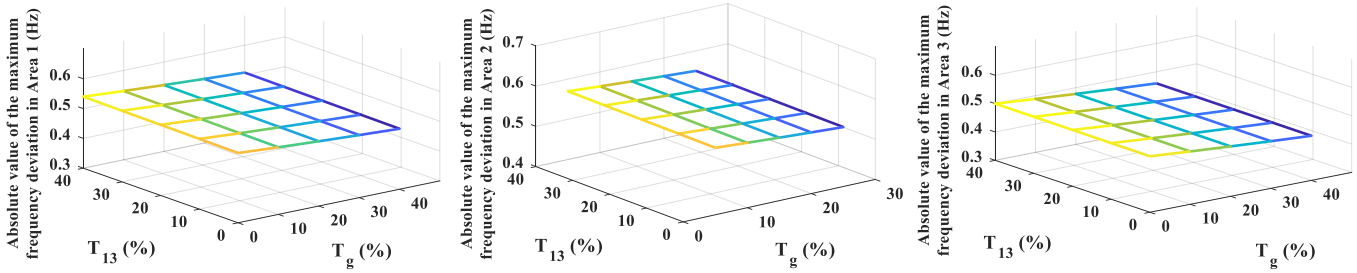

Fig. 9. Impact of changes of T_g and T_{13} on the absolute maximum deviation of frequency responses

In continue, the BEL coordinator is included in the control system. A 0.1 p.u. load change in area 1 and another 0.1 p.u. load change in area 2 are considered. For the rest of the simulations, the communication delay is 1 s. The ACE deviation for the BEL controller with the BEL coordinator between TGUs and IACs aggregators and BEL controller without coordination scheme are plotted in Fig. 12. The attained results prove that the proposed BEL-based coordinator scheme can dramatically mitigate the value of the frequency and tie-line power overshoots and variations in comparison to the BEL based aggregation control without the contribution of the intelligent coordinator and other ones, thus resulting in an ensured performance of the proposed coordinator scheme in the presence of time delay.

D. Comparison with Model-based Control Methods

A model predictive control (MPC) and a linear quadratic regulator (LQR) are used to assess the BEL-based controller

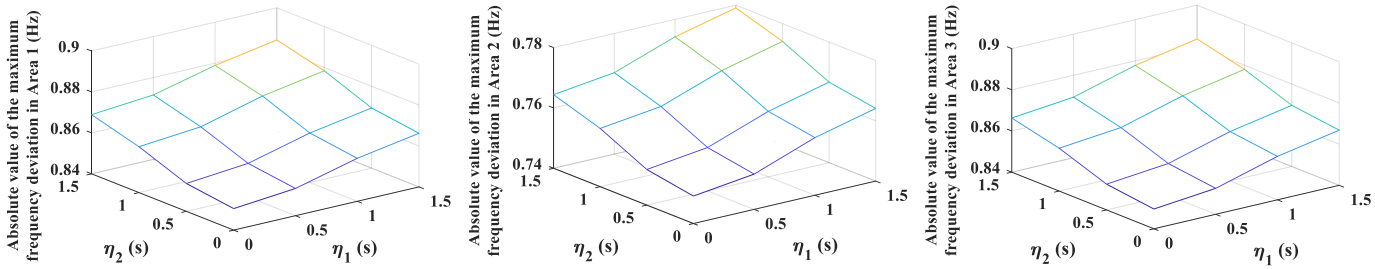

Fig. 10. Impact of varying time delays on the absolute maximum deviation of frequency responses

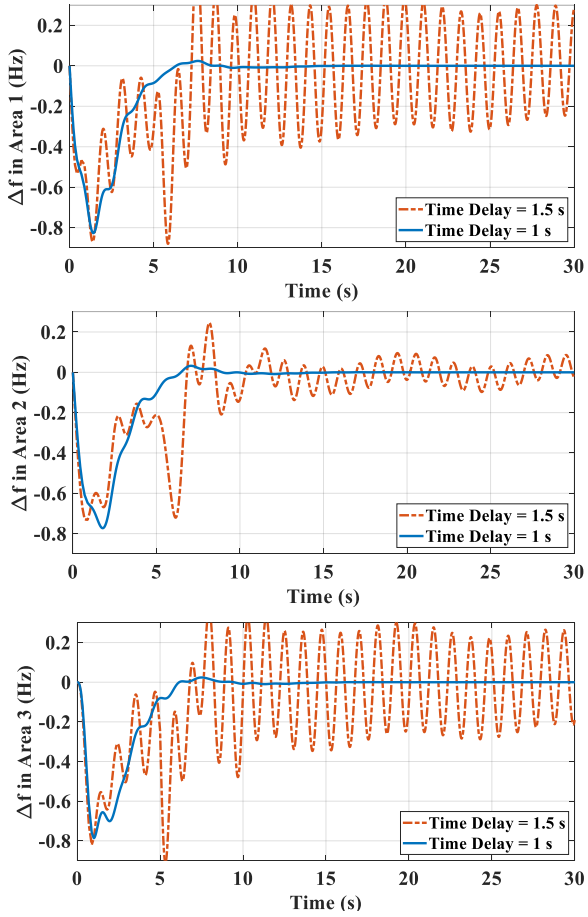

Fig. 11. Deviation in the frequency of areas considering time delays

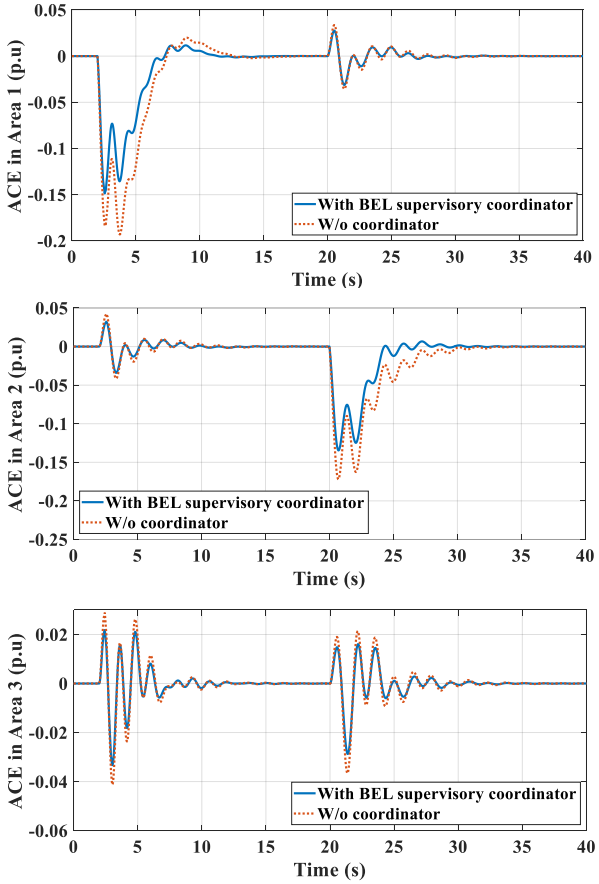

Fig. 12. Dynamic performance of the proposed coordinator

performance. The LQR and MPC fall into group of model-based control algorithms. For the MPC controller design, the control and prediction horizons are chosen as 3 and 10, respectively. For the LQR controller, the control command is generated as $u_{IAC}(t) = -K_L x'(t)$ for a state variable $x' = [\Delta f_i \ \Delta P_{tie-i} \ \Delta P_{IAC,T} \ \Delta P_a \ \Delta P_b]^T$, where K_L is the gain matrix. The control command is computed as follows:

$$\min \int_0^\infty \left({x'}^T W_1 x' + {u_{IAC}}^T W_2 u_{IAC} \right) \mathrm{d}t \qquad (57)$$

where W_1 and W_2 are symmetric positive definite matrices.

In this scenario, it is intended for the TGU to be worked so near to the generation restrictions that it cannot provide an appropriate up/down reserve to keep up with the imposed load change. Model uncertainty is also considered in the tie-line power flow between area 1 and area 2. A uniform disturbance models the uncertainty with upper and lower bounds of 2% to the absolute value of the actual value. The area 1 load increases by 30 MW at t = 2 s, but the TGU can only generate an additional 20 MW of power. In Fig. 13 the results using various control strategies are displayed. As can be seen, the proposed BEL-based controller presents a superior performance over the MPC and LQR-based control schemes. Moreover, nonzero steady-state deviations can be observed in the responses. This results from the fact that the IAC aggregators' regulation capabilities are insufficient to balance the

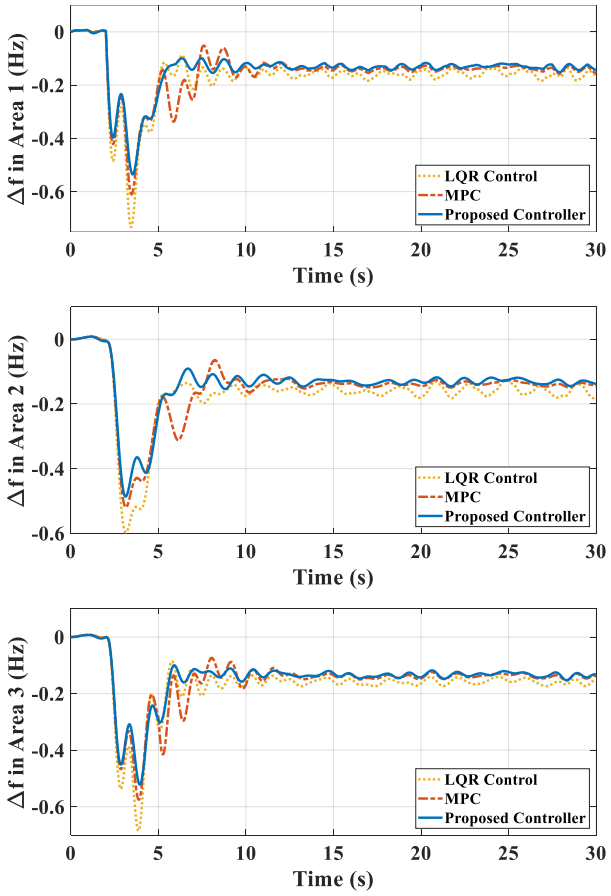

Fig. 13. Comparison between the proposed controller, MPC, and LQR control

reserve shortage. However, compared to the MPC and LQR, the suggested controller's dynamic responses show reduced steady-state variances. For the frequency deviation in areas 1 and 2, where the IAC aggregators are installed, quantitative error indices, including the root mean square (RMS) value and absolute maximum deviation (AMD) are provided. The results are shown in Table IV. As can be seen, by using the proposed BEL-based controller, the AMD value of frequency in area 1 has decreased to 0.5355 Hz from 0.7348 Hz and 0.6105 Hz for the cases that LQR and MPC were used for the IAC aggregators, respectively. In other words, the percentage improvement with the proposed controller in comparison with LQR and MPC is 27.12% and 12.28%, respectively. The table also suggests that the RMS value of deviation has the lowest value when the proposed controller is used. Table V shows the computation time with the applied control methods. Also, it should be stated that the computation burden required by fuzzy-PI control method for this scenario is also included in this table. As the table indicates, the BEL-based controller requires less computational time than MPC, LQR, and fuzzy PI control.

E. Real-time Simulation Results

In order to test the specified power system's applicability and efficiency in real-time, the proposed control and coordination systems are implemented in the OPAL-RT-OP5600 real-time simulator. The general arrangement of the experimental apparatus is shown in Figure 14. An OPAL-RT and a PC make up the setup. The console, slave, and master subsystems are the Simulink model's three divisions used for RT-Lab simulation. The BEL controller and BEL coordinator are executed in the slave subsystem, whereas the master subsystem houses the power grid model. Scopes can be found in the console subsystem as well.

Figure 15 shows how three subsystems are created. The master and slave subsystems are assigned to the same OPAL-RT target, running on separate cores. The sampling time for the real-time testing setup execution of the LFC system with the BEL method is 10 μs. This entails running the test system model, BEL controller, and BEL coordinator. To enable the execution of simulations on a real-time platform, RT-LAB generates the Simulink model's "C" code. A real-time scenario for evaluation of the proposed controller in the control loop of IAC aggregators is utilized. For the simulations, a 0.2 p.u. load change is considered in area 1. The uncertainty is also considered in the tie-line power flow between area 1 and area 2. The comparison results of ACE deviation for the real-time scenario are shown in Fig. 16. The results indicate that the IAC aggregators with the proposed BEL-based controller provide a better dynamic response in terms of peak overshoot and peak undershoot over the fuzzy-PI controller and the method proposed in [15]. The oscilloscope results for different controllers are also plotted in Fig. 17 in a time scale of 20 s. Table VI is also provided to compare the performance indices obtained by the proposed controller, fuzzy-PI, and proportional control methods. As shown, the proposed BEL-based controller provides the lowest values for the error criteria. For example, the percentage improvement with the proposed controller in comparison with a proportional control method reported in [19] in terms of the AMD value of frequency in area 1 is 30%.

TABLE IV
CHARACTERISTIC COMPARISON OF THE PROPOSED CONTROLLER, MPC, AND LQR CONTROL

Controller type	AMD (Hz)		RMS (Hz)	
	Δf_1	Δf_2	Δf_1	Δf_2
Proposed Controller	0.5355	0.4866	0.1760	0.1759
MPC	0.6105	0.5196	0.1938	0.1922
LQR Control	0.7348	0.5976	0.2116	0.2110

TABLE V
COMPARISON OF THE COMPUTATION TIME

Controllers	Proposed controller	MPC	LQR	Fuzzy-PI
Time (s)	14.10	18.32	23.65	32.47

VIII. CONCLUSION

In this paper, a BEL-based controller was proposed to regulate the power outputs of IAC units for efficient participation in the frequency regulation service of a multi-area

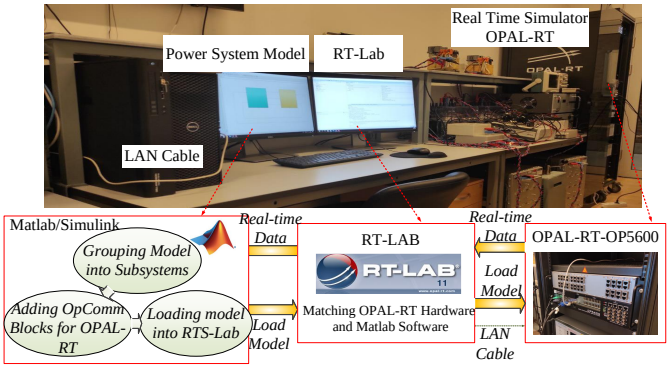

Fig. 14. Real time experimental setup

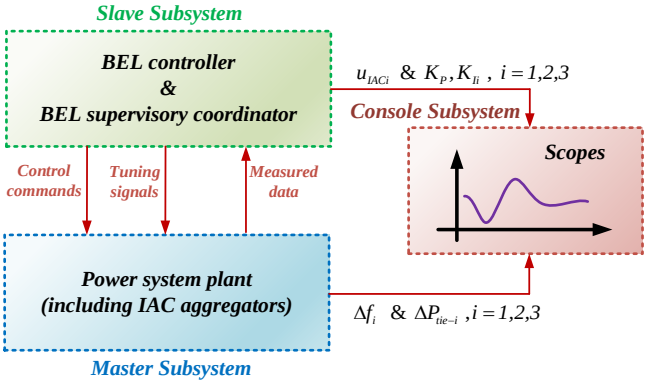

Fig. 15. Schematic view of the master, slave, and console subsystems

TABLE VI
CHARACTERISTIC COMPARISON OF THE PROPOSED CONTROLLER AND FUZZY-PI, AND PROPORTIONAL CONTROL METHODS

Controller type	AMD (Hz)		RMS (Hz)	
	Δf_1	Δf_2	Δf_1	Δf_2
Proposed Controller	0.3122	0.3165	0.0652	0.0647
Fuzzy-PI	0.3672	0.3723	0.0767	0.0762
Proportional Controller [19]	0.4223	0.4282	0.0882	0.0876

power system. The controller was developed to deal with the uncertainties introduced by the system parameters and loads. Its capability was demonstrated in providing effective control commands for the IACs over the other controllers examined. The results showed that the proposed controller performs better regarding the settling time and peak value of the frequency and tie-line deviations. A BEL supervisory coordinator was also developed to overcome the time delay problem in the power system model, particularly the time delays that occurred in the control loop of IACs. The BEL coordinator produced supplementary gains for the PI controller embedded in the control loop of TGUs. The results confirmed that the proposed BEL coordinator could reduce the frequency deviations compared to the scheme without adjustment. Finally, the proposed BEL-based controller was validated by the OPAL-RT real-time simulator. Although this verification was conducted by a load disturbance scenario discussed in Subsection VII-D, it

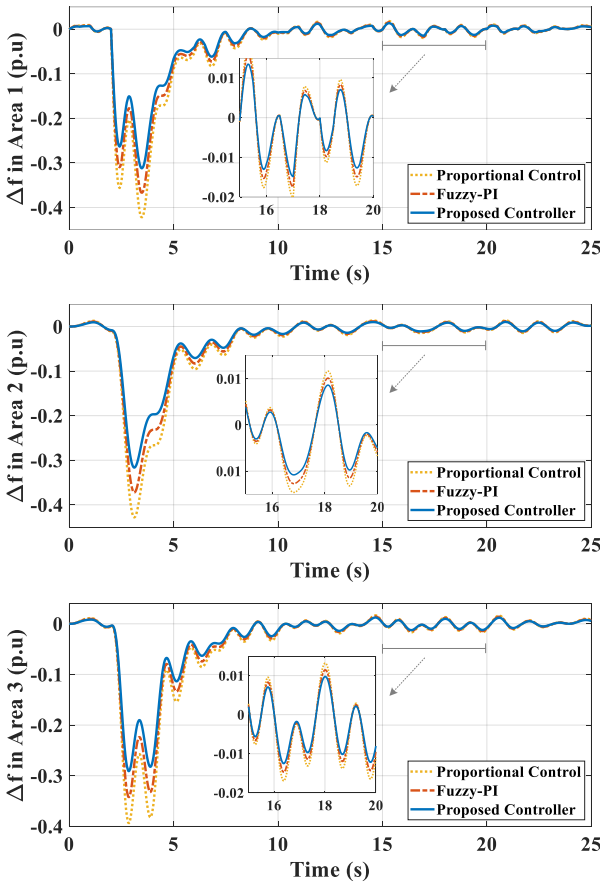

Fig. 16. Dynamic performance of the proposed controller in real-time scenario

could be done for other case studies to assess the regulation performance for different kinds of disturbances in the system and other possible uncertainties discussed in Section VII. In future work, to improve the performance of the BEL-based controller, optimization techniques can be used to specify control parameters precisely.

APPENDIX

Fig. 18 shows the MFs connected to the inputs and outputs. The MFs are grouped into the following categories: negative large (NL), negative small (NS), zero (Z), positive small (PS), and positive large (PL).

REFERENCES

[1] A. Oshnoei et al., "Coordinated control scheme for provision of frequency regulation service by virtual power plants", *Appl. Energy*, vol. 325, pp. 119734, Nov. 2022.
[2] P. Babahajiani, Q. Shafiee, and H. Bevrani, "Intelligent demand response contribution in frequency control of multi-area power systems," *IEEE Trans. Smart Grid*, vol. 9, no. 2, pp. 1282–1291, Mar. 2018.
[3] M. R. Vedady Moghadam, R. T. B. Ma, and Z. Rui, "Distributed frequency control in smart grids via randomized demand response," *IEEE Trans. Smart Grid*, vol. 5, no. 6, pp. 2798–2809, Nov. 2014.
[4] G. Chen, H. Zhang, H. Hui, N. Dai, and Y. Song, "Scheduling thermostatically controlled loads to provide regulation capacity based on a learning-based optimal power flow model," *IEEE Trans. Sustainable Energy*, early access, DOI: 10.1109/TSTE.2021.3100846, 2021.

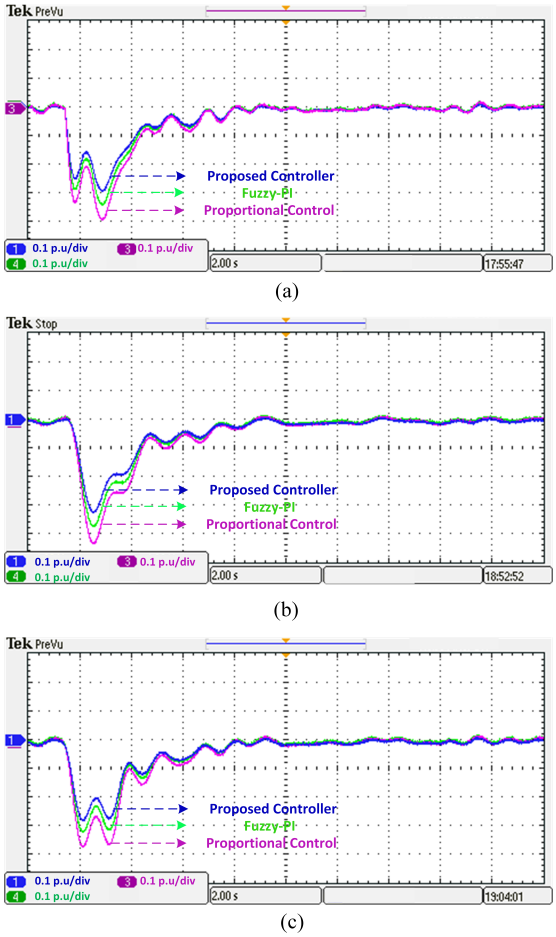

Fig. 17. Digital scope output representing the deviation in the frequency of (a) area1, (b) area 2, (c) area 3

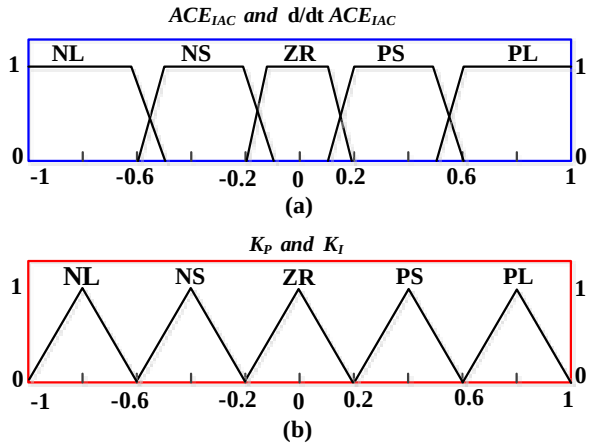

Fig. 18. MFs for (a) inputs and (b) outputs

[5] M. Kuzlu, M. Pipattanasomporn, and S. Rahman, "Hardware demonstration of a home energy management system for demand response applications," *IEEE Trans. Smart Grid*, vol. 3, no. 4, pp. 1704–1711, Dec. 2012.

[6] A. Oshnoei, M. Kheradmandi, S.M. Muyeen, and N.D. Hatziargyriou, "Disturbance Observer and Tube-based Model Predictive Controlled Electric Vehicles for Frequency Regulation of an Isolated Power Grid," *IEEE Trans. Smart Grid.*, vol. 12, no. 5, pp. 4351 –4362, 2021.

[7] A. Oshnoei, R. Khezri, and S.M. Muyeen, "Model predictive-based secondary frequency control considering heat pump water heaters," *Energies*, vol. 12, no. 3, pp. 1–18, 2019.

[8] A. Malik and J. Ravishankar, "A hybrid control approach for regulating frequency through demand response," *Appl. Energy*, vol. 210, pp. 1347–1362, Jan. 2018.

[9] T. Jiang, P. Ju, C. Wang, H. Li, and J. Liu, "Coordinated control of air-conditioning loads for system frequency regulation," *IEEE Trans. Smart Grid.*, vol. 12, no. 1, pp. 548–560, Jan. 2021.

[10] H. Hui, Y. Ding, and M. Zheng, "Equivalent modelling of inverter air conditioners for providing frequency regulation service," *IEEE Trans. Ind. Electron.*, vol. 66, no. 2, pp. 1413–1423, Feb. 2019.

[11] YR. Rodrigues, M, Abdelaziz, L. Wang, and I. Kamwa, "PMU Based Frequency Regulation Paradigm for Multi-Area Power Systems Reliability Improvement," *IEEE Trans. Power Syst.*, vol. 36, no. 5, pp. 4387–4399, Mar. 2021.

[12] A. Oshnoei, M. Kheradmandi, and S. M. Muyeen, "Robust control scheme for distributed battery energy storage systems in load frequency control," *IEEE Trans. Power Syst.*, vol 35, no. 6, pp. 4781–4791, 2020.

[13] W. Cui et al., "Evaluation and sequential dispatch of operating reserve provided by air conditioners considering leadlag rebound effect," *IEEE Trans. Power Syst.*, vol. 33, no. 6, pp. 6935–6950, Nov. 2018

[14] X. Hu, and J. Nutaro, "A priority-based control strategy and performance bound for aggregated HVAC-based load shaping," *IEEE Trans. Smart Grid*, vol 11, no. 5, pp. 4133–4143, 2020.

[15] M. Song, C. Gao, J. Yang, and H. Yan, "Energy storage modeling of inverter air conditioning for output optimizing of wind generation in the electricity market," *CSEE JPES*, vol. 4, no. 3, pp. 305–315, Sep. 2018.

[16] X. Wu, J. He, Y. Xu, J. Lu, N. Lu, and X. Wang, "Hierarchical control of residential HVAC units for primary frequency regulation," *IEEE Trans. Smart Grid*, vol. 9, no. 4, pp. 3844–3856, July. 2018.

[17] W. Mendieta, C. A. Caizares,"Primary Frequency Control in Isolated Microgrids using Thermostatically Controllable Loads," *IEEE Trans. Smart Grid*, vol. 12, no. 1, pp. 93–105, Jan. 2021.

[18] N. Zhao, et al. "Model predictive based frequency control of power system incorporating air-conditioning loads with communication delay." *International Journal of Electrical Power & Energy Systems* pp. 107856, 2022.

[19] H. Hui, Y. Ding, Z. Lin, P. Siano, and Y. Song, "Capacity allocation and optimal control of inverter air conditioners considering area control error in multi-area power systems," *IEEE Trans. Power Syst.*, vol. 35, no. 1, pp. 332–345, Jan. 2020.

[20] H. Hui, Y. Ding, T. Chen, S. Rahman, and Y. Song, "Dynamic and stability analysis of the power system with the control loop of inverter air conditioners," *IEEE Trans. Ind. Electron.*, vol. 68, no. 3, pp. 2725–2736, 2021.

[21] F. Yang et al., "Disturbance Observer based Fractional-order Integral Sliding Mode Frequency Control Strategy for Interconnected Power System," *IEEE Trans. Power Syst.*, early access, DOI: 10.1109/TPWRS.2021.3081737, 2021.

[22] Y. Khayat et al., "Decentralized optimal frequency control in autonomous microgrids," " *IEEE Trans. Power Syst.*, vol. 34, no. 3, pp. 2345–2353, May 2019.

[23] S. Oshnoei, A. Oshnoei, A. Mosallanejad, and F. Haghjoo, "Contribution of GCSC to regulate the frequency in multi-area power systems considering time delays: A new control outline based on fractional order controllers," *International Journal of Electrical Power & Energy Systems*, vol. 123, p. 106197, 2020.

[24] A. Oshnoei, M. Kheradmandi, R. Khezri, and A. Mahmoudi, "Robust model predictive control of gate-controlled series capacitor for LFC of power systems," *IEEE Trans. Ind. Inform.*, vol 17, no. 7, pp. 4766–4776, 2020.

[25] Z. Yan and Y. Xu, "A multi-agent deep reinforcement learning method for cooperative load frequency control of a multi-area power system," *IEEE Trans. Power Syst.*, vol 35, no. 6, pp. 4599–4608, 2020.

[26] C. Lucas, D. Shahmirzadi, and N. Sheikholeslami, "Introducing BELBIC: Brain emotional learning based intelligent controller," *Intell. Automat. Soft Comput.*, vol. 10, no. 1, pp. 11–21, 2004.

[27] M. Saeed, et al., "Semi-active vibration control of building structure by Self Tuned Brain Emotional Learning Based Intelligent Controller," *Journal of Building Engineering*, pp. 103664, 2022.

[28] C.-F. Hsu and T.-T. Lee, "Emotional fuzzy sliding-mode control for unknown nonlinear systems," *Int. J. Fuzzy Syst.*, vol. 19, no. 3, pp. 942–953, 2017.

[29] A. M. Yazdani, A. Mahmoudi, M. Movahed, P. Ghanooni, S. Mahmoudzadeh, and S. Buyamin, "Intelligent speed control of hybrid stepper motor considering model uncertainty using brain emotional learning", *Can. J. Electric. Comp. Eng.*, vol. 41, iss. 2, pp. 95–104, Aug. 2018.

[30] M. S. O. Yeganeh, A. Oshnoei, N. Mijatovic, T. Dragicevic, and F. Blaabjerg, "Intelligent Secondary Control of Islanded AC Microgrids: A Brain Emotional Learning-based Approach," *Accepted to be published in IEEE Trans. Ind. Electron.*, 2022. DOI: 10.1109/TIE.2022.3203677
[31] R. Khezri, A. Oshnoei, A. Yazdani, and A. Mahmoudi, "Intelligent coordinators for automatic voltage regulator and power system stabiliser in a multi-machine power system," *IET Gener. Transm. and Distrib.*, vol. 14, no. 23, pp. 5480–5490, 2020.
[32] M. A. Rahman, R. M. Milasi, C. Lucas, B. N. Arrabi, and T. S. Radwan, "Implementation of emotional controller for interior permanent magnet synchronous motor drive," *IEEE Trans. Ind. Appl.*, vol. 44, no. 5, pp. 1466–1476, Oct. 2008.
[33] E. Daryabeigi, A. Mirzaei, H. A. Zarchi, and S. Vaez-Zadeh, "Enhanced emotional and speed deviation control of synchronous reluctance motor drives," *IEEE Trans. Energy Convers.*, vol. 34, no. 2, pp. 604–612, Jun. 2019.
[34] W. Cui et al., "Evaluation and sequential dispatch of operating reserve provided by air conditioners considering leadlag rebound effect," *IEEE Trans. Power Syst.*, vol. 33, no. 6, pp. 6935–6950, Nov. 2018.
[35] M. Shafie-khah and P. Siano, "A stochastic home energy management system considering satisfaction cost and response fatigue," *IEEE Trans. Ind. Inform.*, vol. PP, no. 99, pp. 629–638, July 2017.
[36] A. Ameli, A. Hooshyar, E. El-Saadany, and A. Youssef, "Attack detection and identification for automatic generation control systems," *IEEE Transactions on Power Systems*, 2018.
[37] M. Vrakopoulou, P. M. Esfahani, K. Margellos, J. Lygeros, and G. Andersson, "Cyber-attacks in the automatic generation control," in Cyber Physical Systems Approach to Smart Electric Power Grid. Springer, 2015, pp. 303–328.
[38] B. Debnath and S. J. Mija, "Emotional learning based controller for quadruple tank systemAn improved stimuli design for multiple setpoint tracking," *IEEE Trans. Ind. Electron.*, vol. 68, no. 11, pp. 11296–11308, 2020.
[39] S. Oshnoei, A. Oshnoei, A. Mosallanejad, and F. Haghjoo, " Novel load frequency control scheme for an interconnected two-area power system including wind turbine generation and redox flow battery," *Int. J. Electr. Power Energy Syst.*, vol. 130, p. 107033, 2021.
[40] M. Datta, T. Senjyu, "Fuzzy control of distributed PV inverters/energy storage systems/electric vehicles for frequency regulation in a large power system," *IEEE Trans. Smart Grid.*, vol. 4, no. 1, pp. 479–488, 2013.
[41] N. Pathak and Z. Hu, "Hybrid-peak-area-based performance index criteria for AGC of multi-area power systems," *IEEE Trans. Ind. Informat.*, vol. 15, no. 11, pp. 5792–5802, Nov. 2019.